9 Sensitivity Analysis and Uncertainty Quantification of a Single Combusting Particle

Ahmed Hassan and Taraneh Sayadi

Contents

Abstract

This study explores the complex phenomena involved in simulations of unsteady solid fuel particle combustion. These simulations use models that depend on parameters from experiments or small-scale simulations, making it important to quantify the sensitivities and uncertainties of predicted quantities. The study

A. Hassan (✉) · T. Sayadi
Institute for Combustion Technology, RWTH Aachen University, Aachen, Germany
e-mail: a.hassan@itv.rwth-aachen.de

T. Sayadi
e-mail: taraneh.sayadi@lecnam.net

R. Kneer et al. (eds.), *Clean Energy Conversion*,
https://doi.org/10.1007/978-3-031-98956-8_9

focuses on combustion under different freestream compositions, such as air and oxy-fuel atmospheres. The first step involves identifying the most sensitive model parameters, a process developed in a previous study. The framework is extended to study the evolution of sensitivities over time for a single unsteady particle undergoing devolatilisation. The dominant model parameters affecting particle temperature and burning rate are identified for both air and oxy-fuel atmospheres. The impact of different devolatilisation models on sensitivities is also examined. Additionally, an adjoint-based active subspace method (AASM) is employed to quantify uncertainties in predictions. The results show that uncertainties in particle parameters are much greater than those in gas-phase reaction rates. Furthermore, uncertainties are larger in oxy-fuel atmospheres than in air, emphasising the effect of freestream composition on model predictions.

9.1 Introduction

As demonstrated in this book, the new solid fuel sources require careful modelling of the combustion process as it occurs in the solid particle as well as its interaction with the surrounding gas. To this end, experimental campaigns have been undertaken in order to characterise and model the existing heterogeneous and homogeneous reactions. Numerical investigations using the developed models, such as char burnout, devolatilisation and gas-phase reactions, are then used to predict the overall efficiency of the underlying system. As the models used in these simulations are developed through experiments, they are reported with a confidence range (i.e. probabilistic variables) and therefore the predictions of the models need to be assessed in terms of the existing uncertainties. This information would be an indication of the robustness of the predictions of the simulations. In this chapter, dedicated methods to extract such sensitivities and uncertainties in the predictions with respect to the combustion model parameters are presented, both in the solid particle and in the gas phase.

The most common method for calculating the gradient of various objective functions with respect to model parameters is forward sensitivity estimation. However, as can be seen from the work presented in this book, the size of the parameter space (i.e. the number of parameters representing the kinetic models) makes the forward approach prohibitively expensive. An alternative approach is the adjoint-based method. This method is an efficient alternative to extract the sensitivities of relevant quantities of interest (QoI): The performance of the adjoint-state method does not depend on the number of parameters and is easily applicable to unsteady configurations. The application of the adjoint-state method in fluid mechanics dates back to the pioneering work by Pironneau [1], followed by Jameson et al. [2] with application to aeronautical shape optimisation. Since then adjoint-based techniques have been used for optimal control of non-linear problems [3], and in particular, in the combustion community, to study ignition delay time of zero-dimensional reactors [4], steady-state flames [5], and more recently, to high-fidelity turbulent reacting

flow [6]. For multiphase combustion (solid/gas), the adjoint-state method to steady and unsteady char combustion is applied [7,8].

Based on this methodology, the analysis of more sophisticated combustion models is presented in this chapter. More importantly, the variations in the sensitivities of the most dominant parameters over time are also studied. The results of this investigation will be important for transient problems such as that of single particle combustion, which can go through different stages of combustion from degassing, ignition and char burnout. This strategy will allow to determine whether any of the existing physical phenomena can cause a significant change in the evolution of sensitivities.

While informative in identifying the sensitive parameters in the model, sensitivity analysis provides only a local estimate of the variation in the quantity of interest with respect to each parameter. To gain a global perspective, it is necessary to perform uncertainty quantification. Traditional methods for performing uncertainty quantification (UQ), such as Monte-Carlo, become infeasible when dealing with systems with a large parameter space (curse of dimensionality). Therefore, several stochastic models have been proposed, such as polynomial chaos expansion (PCE) [9], as well as other techniques that consider only a small part of the parameter space to make the analysis affordable. Alternative methods to reduce computational time are high dimensional model representations (HDMR) [10] and artificial neural networks (ANN) [11]. Despite ongoing efforts to overcome the curse of dimensionality, these methods become inefficient as the number of parameters increases. As an alternative, the active subspace method (ASM) has been proposed [12] to identify the key directions in the function space of the QoI, allowing for a more efficient analysis. ASM has been applied to several studies in the field of combustion, proving to be a successful framework for quantifying uncertainties in various reactive configurations with a large number of parameters [13,14]. The ASM method has been successfully combined with the adjoint state method to further reduce the cost of the algorithm and improve its efficiency by increasing the accuracy of the extracted gradients [15,16]. The technique is called the adjoint active subspace method (AASM).

In addition, an alternative method using only the adjoint information, called the linear approximation adjoint-based method (LAAM) is proposed, to approximate the resulting uncertainties. A comparison of this strategy with the state-of-the-art in the context of a zero-dimensional reactor (Table 9.1) shows that the cost of LAAM is generally about two orders of magnitude lower than that of ASM. The computational cost of ASM compared to LAAM increases significantly as the size of the considered chemical kinetic mechanism increases. This remarkable cost reduction highlights the advantage of LAAM, especially as a first estimation of the uncertainties of large mechanisms.

The resulting algorithm is also implemented in the open-source package `Apophis.jl`. The package is coded in the Julia language. It is important to note that Julia is a new programming language designed to facilitate the computation of scientific applications. Julia combines the execution speed of statically typed languages with the active performance of dynamic languages. This package provides the community with a framework for investigating the uncertainties of chemical kinetic models in an isochoric adiabatic reactor configuration.

Table 9.1 Comparison of LAAM to ASM for various gas-phase mechanisms. For more information regarding the mechanisms the reader is referred to Hassan et al. [15].

Mechanism	h2vb	GRI 1.2	GRI 2.11	GRI 3.0	ITV
# Species	10	32	49	53	490
# Reaction	21	177	297	325	2072
Time (LAAM) [s]	160×10^{-3}	2.6	6	15	2268
Time (ASM) [s]	50	1203	3716	11571	2.5×10^{6}

Despite the successful use of AASM and LAAM to extract model parameter uncertainties, the above-mentioned contribution only studied simple configurations in unsteady zero-dimensional or steady one-dimensional settings. Additionally, previous studies on sensitivities of solid fuel combustion also considered char models only, neglecting important phenomena such as devolatilisation. Thus, in what follows: (i) the evaluation of the effectiveness of adjoint-based methods and AASM in extracting sensitivities and uncertainties in more complex unsteady systems, including devolatilisation, (ii) the identification of the most significant gas-phase reactions by incorporating detailed gas-phase combustion mechanisms, and (iii) the examination of the effect of freestream composition on the extracted sensitivities and uncertainties.

This chapter is structured as follows: Sect. 9.2 briefly introduces the underlying configuration and the models used to represent the reaction in the particle and gas phases, as well as the respective freestream compositions. The simulations of unsteady axisymmetric particle are then presented and discussed in Sect. 9.3. Section 9.4 discusses the methodology used to extract the sensitivities and discusses the extracted sensitivities for the different quantities of interest with respect to the existing modelling parameters. The evolution of the important sensitivities over time is also presented and discussed in Sect. 9.5. Section 9.6 presents the AASM algorithms and the results of the uncertainty quantification for different model parameters. The temporal evolution of the extracted uncertainties is also discussed. Finally, Sect. 9.7 discusses the summary and conclusion of this work.

9.2 Models and Configuration

The configuration considered here is a reactive axisymmetric particle in a fluid, as shown in Fig. 9.1.

9.2.1 Governing Equations

The governing equations that describe the flow around a reactive axisymmetric particle in a fluid are presented in a similar way as in the study by Hassan et al. [8]:

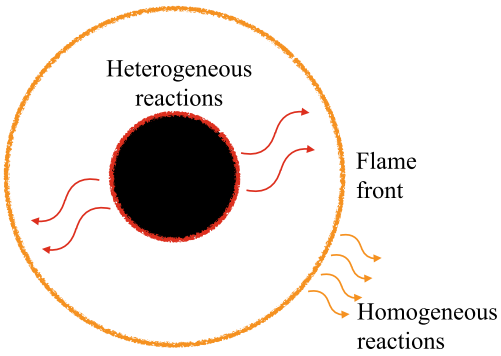

Fig. 9.1 Schematic of an axisymmetric configuration used in this chapter

$$\frac{\partial \rho}{\partial t} + \frac{1}{r^\alpha}\frac{\partial}{\partial r}\left(\rho\, r^\alpha\, u\right) = 0, \tag{9.1}$$

$$\frac{\partial(\rho\, Y_i)}{\partial t} + \frac{1}{r^\alpha}\frac{\partial}{\partial r}\left[\rho\, r^\alpha \left(u\, Y_i - D_i \frac{\partial Y_i}{\partial r}\right)\right] - \omega_i = 0, \tag{9.2}$$

$$c_{\mathrm{p}}\frac{\partial(\rho\, T)}{\partial t} + \frac{c_p}{r^\alpha}\frac{\partial}{\partial r}\left[\rho r^\alpha \left(u\, T - \frac{\lambda}{c_p}\frac{\partial T}{\partial r}\right)\right] + \sum_{i=1}^{N_{\mathrm{s}}} h_i\, \omega_i = 0, \tag{9.3}$$

where t and r are the independent variables, $i = 1, \ldots, N_{\mathrm{s}}$ denotes the species and $\alpha = 2$ for spherical coordinates. The diffusion model is based on Fick's law, and Fourier's law has been used to model heat transfer. Also, c_p denotes the thermal capacity of the mixture at constant pressure, λ its heat conductivity, and D_i is the diffusion coefficient of species i. The mixture density is denoted by ρ, and the radial mass-centred velocity is u. The mass fractions and temperature are denoted as Y_i and T, respectively. In (9.3), the term $\sum h_i\, \omega_i$ represents the heat release due to chemical reactions, where h_i denotes the specific enthalpy and ω_i denotes the production rate of the i^{th} species.

Mass-Based Coordinates

For ease of implementation, and without loss of generality, the governing equations can be mapped from the physical coordinates (r, t) to the mass-based coordinate system (ψ, τ). This transformation satisfies the continuity equation by introducing a new algebraic equation in which the discrete form of the mapping equation has a closed-form solution. Moreover, the direct dependency on the velocity variable is eliminated from the governing equations. The transformation is carried out using (9.4) and (9.5):

$$\frac{\partial}{\partial r} = \rho\, r^2\, \frac{\partial}{\partial \psi}, \tag{9.4}$$

$$\frac{\partial}{\partial t} = \frac{\partial}{\partial \tau} - \rho\, r^2\, u_r \frac{\partial}{\partial \psi} + \dot{m}_0^\alpha \frac{\partial}{\partial \psi} \tag{9.5}$$

where $\dot{m}_0^{\alpha}$ represents the mass flux per unit surface area. Applying chain rule to (9.4) and (9.5), under the assumption of unity Lewis number, yields to (9.6) and (9.7) that govern the evolution of species and energy in the transformed coordinates:

$$\frac{\partial Y_i}{\partial \tau} + \dot{m}_0^{\alpha} \frac{\partial Y_i}{\partial \psi} - \frac{\partial}{\partial \psi}\left(\rho r^{2\alpha} \frac{\lambda}{c_{\mathrm{p}}} \frac{\partial Y_i}{\partial \psi}\right) - \frac{\omega_i}{\rho} = 0, \tag{9.6}$$

$$\frac{\partial T}{\partial \tau} + \dot{m}_0^{\alpha} \frac{\partial T}{\partial \psi} - \frac{\lambda}{c_p} \frac{\partial}{\partial \psi}\left(\rho\, r^{2\alpha} \frac{\partial T}{\partial \psi}\right) + \frac{1}{\rho\, c_p} \sum_{i=1}^{N_{\mathrm{s}}} h_i\, \omega_i = 0, \tag{9.7}$$

where r is computed from the following equation, which in turn enforces mass conservation:

$$\frac{\partial r}{\partial \psi} = \frac{1}{\rho\, r^2}. \tag{9.8}$$

9.2.2 Boundary Conditions and Freestream Compositions

The first set of boundary conditions at the particle surface balances the mass transfers from the solid phase and the gas phase, which are due to phase change from solid to gas, resulting from devolatilisation and surface reactions. They take the form of coupled Robin boundary conditions and, once recast in the transformed coordinate system, read as

$$\dot{M}_{\mathrm{s}}\, Y_{i,\mathrm{s}} - \mathrm{C}_{\alpha}\, \rho\, r_0^{2\alpha} \frac{\lambda}{c_{\mathrm{p}}} \left.\frac{\partial Y_i}{\partial \psi}\right|_{\mathrm{s}} - \omega_{i,\mathrm{s}} = 0 \tag{9.9}$$

where $\mathrm{C}_{\alpha} = 4\pi$. The variables associated with the particle surface are annotated with the subscript "s". The burning rate $\dot{M}_{\mathrm{s}}$ is the sum of the char reaction rate and the volatile release rate, which can be expressed as:

$$\dot{M}_{\mathrm{s}} = \dot{m}_{\mathrm{c}} + \sum_{i=1}^{N_{\mathrm{v}}} \dot{m}_{\mathrm{v},i} \tag{9.10}$$

where $\dot{m}_{\mathrm{c}}$ is the char burning rate, $\dot{m}_{\mathrm{v},i}$ is the volatile mass release rate of species i, and $\omega_{i,\mathrm{s}}$ is the total chemical source of species i at the particle surface. Assuming thermal equilibrium between the particle surface and the adjacent gas-phase layer, the gas-phase temperature at the particle surface ($T_{\mathrm{s}}^{\mathrm{g}}$) matches the particle temperature (T_{p}),

$$T_{\mathrm{s}}^{\mathrm{g}} = T_{\mathrm{p}}. \tag{9.11}$$

The particle temperature is in turn evaluated by stating the energy conservation in a spherical control volume delimited by the particle surface

$$M_{\mathrm{p}}\, C_{\mathrm{s}} \frac{\partial T_{\mathrm{p}}}{\partial \tau} - \mathrm{C}_{\alpha}\, \rho\, r_0^{2\alpha}\, \lambda_{\mathrm{s}} \frac{\partial T}{\partial \psi} - \left(\sum_{i=1}^{\mathrm{N}} \dot{m}_{\mathrm{v},i}\, h_{\mathrm{v},i} + \dot{m}_{\mathrm{c}}\, h_{\mathrm{c}}\right) = 0, \tag{9.12}$$

Table 9.2 Compositions of oxygen-rich air and oxy-fuel atmospheres.

Test case	Diluent	$Y^{\infty}_{O_2}$ [%]	Y^{∞}_{CO} [%]	$Y^{\infty}_{CO_2}$ [%]	$Y^{\infty}_{N_2}$ [%]	T^{∞} [K]
Air	N_2	32.6	0	10.5	56.9	1673
Oxy-fuel	CO_2	26.2	0	73.8	0	1673

where M_p, C_s, and λ_s are the particle mass, heat capacity and heat conductivity, respectively. The enthalpy of the char reaction h_c and the devolatilisation $h_{v,i}$ will be discussed in Sect. 9.2.3 together with the different source terms. The thermodynamic properties of the particle are taken from Hassan et al. [8]. The variation in the particle mass due to combustion and devolatilisation can be computed as

$$\frac{dM_p}{dt} = -\dot{M}_s \tag{9.13}$$

Finally, the boundary conditions in the far-field are set to the following Dirichlet conditions:

$$Y_i\,(\tau, \psi \to \infty) = Y_i^{\infty}, \tag{9.14}$$

$$T\,(\tau, \psi \to \infty) = T^{\infty}. \tag{9.15}$$

The compositions considered in this study are presented in Table 9.2, and are similar to those of Farmand et al. [17] and Farazi et al. [18].

9.2.3 Chemical and Thermodynamic Models

Several terms introduced in (9.9)–(9.12) require modelling. In this section, the chemical and thermodynamic models used to closed the above system are discussed.

Char Combustion

To model the char burning rate, a single-step reaction is considered with the reaction

$$C(s) + O_2(g) \to CO_2(g). \tag{9.16}$$

The char burning rate, denoted as $\dot{m}_c$, is modelled as the rate of oxygen consumption at the particle surface. This can be expressed as:

$$\dot{m}_c = \omega_{O_2,s} = \rho_c\, K_c\, Y_{O_2,s}\, \pi\, d_p^2, \tag{9.17}$$

where ρ_c is the particle density, K_c is the char reaction rate, $Y_{O_2,s}$ is the oxygen mass fraction at the particle surface, and $d_p = 120\ \mu m$ is the particle diameter. The char reaction rate is computed using Arrhenius law with $E_c = 100.9\ kJ\ mol^{-1}$, $\beta_c = 0$ and $A_c = 3020.75\ s^{-1}$. Finally, the heat of reaction is $h_c = 3 \times 10^4\ kJ\ kg^{-1}$, following the model described in the study by Du and Annamalai [19].

Table 9.3 Volatile species composition.

Species	H	CO	CO_2	CH_4
Composition [%]	32.6	0	10.5	56.9

Devolatilisation
A two-step reaction model [17,19] with first-order kinetics is used to represent the mass release of devolatilised species, given by

$$\dot{m}_{\mathrm{v},i} = \zeta_i \, K_{\mathrm{v},i} \, M_{\mathrm{p}}, \tag{9.18}$$

where $\zeta_1 = \zeta_2 = 0.5$ are the release constants. The volatile release rate $K_{\mathrm{v},i}$ follows the Arrhenius law, with the rate constant values for the multiple steps given by $E_{\mathrm{v},1} = 74.1$ kJ mol^{-1}, $A_{\mathrm{v},1} = 1.34 \times 10^5$ s^{-1}, $\beta_{\mathrm{v},1} = 0$, $E_{\mathrm{v},2} = 251$ kJ mol^{-1}, $A_{\mathrm{v},2} = 1.46 \times 10^5$ s^{-1} and $\beta_{\mathrm{v},2} = 0$. The heat release associated with devolatilisation is $h_{\mathrm{v},1} = h_{\mathrm{v},2} = 1 \times 10^3$ kJ kg^{-1} [19]. The species composition resulting from devolatilisation processes is listed in Table 9.3.

Gas-Phase Kinetics
The gas-phase chemistry is presented by the GRI 1.2 mechanism which includes 177 reactions between 32 species. The different thermodynamic properties for each species are computed using NASA polynomial correlations [20] and averaged over the composition as:

$$\Phi = \frac{\phi_i \, Y_i}{\mathrm{W_i}}, \tag{9.19}$$

where $\phi_i \in \{c_{p,i}, h_i, s_i\}$ represents any thermodynamic specific quantity of the i^{th} species. The corresponding mixture average quantity is denoted as Φ. Finally, the closure is completed using the ideal gas law.

9.3 Simulations of an Axisymmetric Solid Particle

The combination of the models and governing equations results in the solutions demonstrated in Fig. 9.2 for the dominant species. As shown in Fig. 9.2a, carbon dioxide peaks away from the particle surface. This can be attributed to the high reactivity of the reaction involving $\mathrm{OH} + \mathrm{CO} \rightleftharpoons \mathrm{H} + \mathrm{CO_2}$, which leads to the consumption of carbon monoxide and the production of carbon dioxide. It should be emphasised that during this phase, char combustion, also known as the heterogeneous ignition, is negligible due to the unavailability of oxygen at the particle surface. This is due to the fact that oxygen is consumed in gas-phase reactions during the devolatilisation process.

As quantities of interest, burning rate and particle temperature are considered and shown in Fig. 9.3. It is essential to identify different stages of temporal evolution of quantities of interest such as burning rate and particle temperature [8].

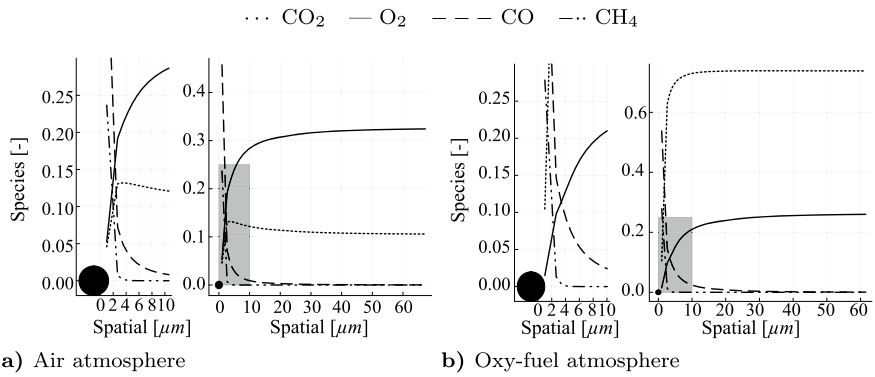

Fig. 9.2 Distribution of species in air and oxy-fuel atmospheres at $t = 4$ ms (reprinted from Hassan et al. [16], Copyright (2024), with permission from Elsevier and minor editing)

These quantities will later be used to characterise parametric sensitivities. As these QoI indicate the different stages of particle combustion (preheating, devolatilisation, ignition, etc.), they help to study the mutual effects and transitions between different phenomena. Additionally, particle temperature is a major parameter measured in different experiments, and can be used to compare and validate numerical results against experimental data [21]. In both the air and oxy-fuel environments, the particle temperature T_p increases due to the temperature gradient between the hot medium and the colder particle. During the initial heating stage ($t < 0.5$ ms), both cases experience similar heating rates due to the significant temperature difference between the gas and solid phases, as depicted in Fig. 9.3a. However, the heating rate for the air atmosphere is lower than that of the oxy-fuel atmosphere due to the more rapid increase in gas-phase temperature for oxy-fuel relative to air. An inflection point can be observed in the T_p evolution curve in Fig. 9.3a around $t \approx 6$ μs,

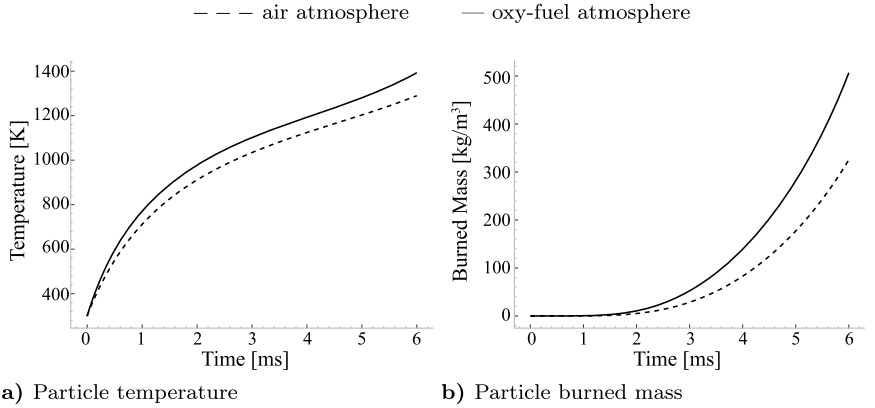

Fig. 9.3 Temporal evolution of particle temperature and burning rate (reprinted from Hassan et al. [16], Copyright (2024), with permission from Elsevier and minor editing)

which is related to the initiation of char ignition. Notably, the inflection point is not observed for the air atmosphere due to the lower particle heating rate.

9.4 Sensitivity Analysis

This section aims to compute the sensitivities of various quantities of interest (QoI) with respect to different model parameters. The gradients will be computed for both the air and oxy-fuel atmospheres, whose compositions are presented in Table 9.2. Additionally, the evolution of sensitivities in time will be examined. All the sensitivities are normalised, helping to distinguish the dominant parameters.

Sensitivity analysis is a method that enables the determination of the rate of change of a particular output measure, such as burning rate or particle temperature, with respect to various model parameters (thermal conductivity, reaction rates, etc.) or initial conditions. By examining the parameter sensitivities obtained, one can identify the most influential parameters for the accurate evaluation of the quantity of interest. Due to the advantages of the adjoint-based algorithms, as highlighted in the introduction of this chapter, they provide an economical and accurate alternative to existing approaches such as finite difference or forward estimation method. Using adjoint-based strategies, the computational cost scales with the number of quantities of interests as opposed to the number of system variables. In other words, the gradient with respect to all systems parameters can be evaluated in a single (forward then backward) simulation, making this method very attractive in cases with a large parameter space, as is the case of interest in this study [8,15].

Adjoint equations can be derived in various ways: continuous, discrete, or semi-discrete. In this study, the focus will be on the semi-discrete approach, where the adjoint operators are directly extracted for the spatial operators, whereas the time variable is kept continuous. Taking a general form of the system equation in temporally continuous form gives

$$\begin{cases} \frac{\mathrm{d}\mathbf{u}^d}{\mathrm{d}\tau}(\tau) = \mathbf{F}^d\left[\tau, \mathbf{u}^a(\tau), \mathbf{u}^d(\tau), \mathbf{p}\right], \\ \mathbf{0} = \mathbf{F}^a\left[\tau, \mathbf{u}^a(\tau), \mathbf{u}^d(\tau), \mathbf{p}\right], \end{cases} \tag{9.20}$$

where $\mathbf{u} = \left(\mathbf{u}^a, \mathbf{u}^d\right)$ denotes the state vector. This system of equations is in the form of a differential algebraic equation (DAE) system of index 1, thus the state vector consists of differential $\mathbf{u}^d$ (species mass fraction, gas-phase temperature, particle temperature, and particle mass) and algebraic $\mathbf{u}^a$ (mass fractions at the surface) variables. The vector of the chosen parameters is denoted $\mathbf{p}$. The operator $\mathbf{F}^a$ contains the discrete form of the algebraic equations (i.e. Robin boundary and Dirichlet boundary conditions). Similarly, $\mathbf{F}^d$ presents the semi-discrete differential equations and particle temperature equations. It should be stressed that the DAE of index-1 behaves differently from ordinary differential equations (ODE) in that no rate of change of the algebraic variable $\mathbf{u}^a$ appears in the system. After discretising the spatial operators of the forward problem, the first step in deriving the adjoint equations is to form the

following Lagrangian functional

$$L = \mathrm{QoI}\left(\mathbf{u}^a, \mathbf{u}^d, \mathbf{p}\right) - \int_0^{\mathcal{T}} \boldsymbol{\eta}^d \cdot \left\{ \frac{\mathrm{d}\mathbf{u}^d}{\mathrm{d}\tau} - \mathbf{F}^d \left[\tau, \mathbf{u}^a\left(\tau\right), \mathbf{u}^d\left(\tau\right), \mathbf{p}\right] \right\} \mathrm{d}\tau + \int_0^{\mathcal{T}} \boldsymbol{\eta}^a \cdot \mathbf{F}^a \left[\tau, \mathbf{u}^a\left(\tau\right), \mathbf{u}^d\left(\tau\right), \mathbf{p}\right] \mathrm{d}\tau, \quad (9.21)$$

where $\mathcal{T}$ is the time horizon under consideration, and η^a and η^d are the algebraic and differential Lagrangian (adjoint) variables, respectively. The derivation of the adjoint equations changes based on the type of QoI (integral or local [8]). In this study, the interest lies in an average of the QoI in time, written in integral form as

$$\mathrm{QoI} = \int_0^{\mathcal{T}} g\left[\tau, \mathbf{u}^a\left(\tau\right), \mathbf{u}^d\left(\tau\right), \mathbf{p}\right] \mathrm{d}\tau. \quad (9.22)$$

Here g represents the time varying quantity of interest such as particle temperature or burning rate. Substituting this QoI in the Lagrangian functional from (9.21) leads to the following adjoint equations

$$\frac{\mathrm{d}\boldsymbol{\eta}^d}{\mathrm{d}\tau} + \left(\frac{\partial \mathbf{F}^d}{\partial \mathbf{u}^d}\right)^{\dagger} \boldsymbol{\eta}^d + \left(\frac{\partial \mathbf{F}^a}{\partial \mathbf{u}^d}\right)^{\dagger} \boldsymbol{\eta}^a = -\frac{\partial g}{\partial \mathbf{u}^d}, \quad (9.23)$$

$$\left(\frac{\partial \mathbf{F}^d}{\partial \mathbf{u}^a}\right)^{\dagger} \boldsymbol{\eta}^d + \left(\frac{\partial \mathbf{F}^a}{\partial \mathbf{u}^a}\right)^{\dagger} \boldsymbol{\eta}^a = -\frac{\partial g}{\partial \mathbf{u}^a}, \quad (9.24)$$

where † denotes the transpose operator. In this case, the initial condition of the adjoint equation is

$$\boldsymbol{\eta}^d\left(\mathcal{T}\right) = \mathbf{0}. \quad (9.25)$$

The sensitivities can then be evaluated by extracting the gradient of the Lagrangian with respect to the system parameters $\mathbf{p}$. This leads to

$$\frac{\mathrm{dQoI}}{\mathrm{d}\mathbf{p}} = \int_0^{\mathcal{T}} \left(\frac{\partial g}{\partial \mathbf{p}} + \boldsymbol{\eta}^d \cdot \frac{\partial \mathbf{F}^d}{\partial \mathbf{p}} + \boldsymbol{\eta}^a \cdot \frac{\partial \mathbf{F}^a}{\partial \mathbf{p}} \right) \mathrm{d}\tau. \quad (9.26)$$

For a detailed derivation of (9.26), the reader is referred to the study by Hassan et al. [8].

9.4.1 Sensitivities of Particle Temperature

To evaluate sensitivities over all combustion phases and to avoid the complexities of particle ignition, the time-cumulative particle temperature T_p is examined rather than its instantaneous value, resulting in

$$\mathrm{QoI} = \frac{1}{\mathcal{T} - \tau_0} \int_{\tau_0}^{\mathcal{T}} T_\mathrm{p}\, d\tau. \quad (9.27)$$

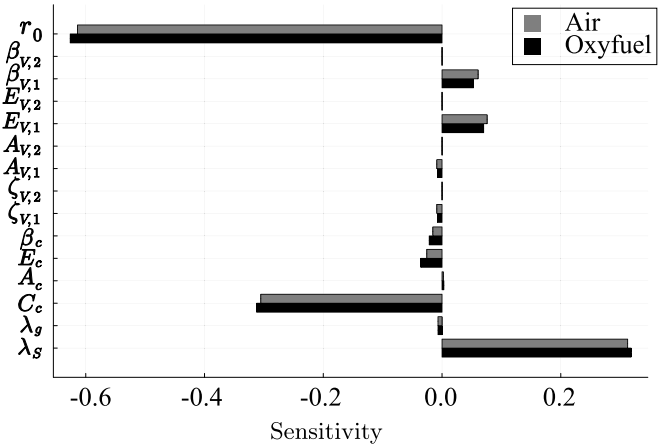

Fig. 9.4 Sensitivity of the average particle surface temperature with respect to the particle parameters, for air and oxy-fuel atmospheres (reprinted from Hassan et al. [16], Copyright (2024), with permission from Elsevier and minor editing)

The integration limits in (9.27) are $\tau_0 = 0$ and $\mathcal{T} = 5$ ms chosen to ensure that gas-phase ignition occurs in both air and oxy-fuel atmospheres, while avoiding char combustion.

The sensitivities of particle temperature with respect to different particle (surface) parameters are shown in Fig. 9.4. It shows that particle size is the most influential parameter, where increasing particle size results in lower temperatures. Sensitivities to particle thermodynamic parameters (C_c and λ_s) are the most prominent during the heat-up phase. Sensitivities with respect to char combustion parameters E_c, β_c and A_c are insignificant due to the absence of heterogeneous ignition. Oxygen is mainly consumed by gas-phase combustion. Particle temperature also shows low sensitivities with respect to various devolatilisation parameters. These parameters are however important when considering particle burning rate, as demonstrated in the study by Farazi et al. [18] and subsequently gas-phase ignition, and will be highlighted in the following section. Comparing sensitivities in air and oxy-fuel atmospheres reveals a similar pattern for both. Notably, the sensitivity to particle parameters r_0, C_c and λ_s are slightly lower in air atmosphere due to weak flammability, where the temperature gradient between gas and particle decreases.

To assess the effect of the mechanism used to model the gas-phase chemistry on the extracted sensitivities, a simpler reduced kinetics mechanism (DRM22), consisting of 104 reactions and 22 species, is implemented in the simulation. The sensitivities of the particle temperature with respect to the different gas-phase reaction rates are shown in Fig. 9.5. A comparison with results from the detailed mechanism shows that the top ten most sensitive reactions are indeed the same in both cases. The first two dominant reactions in air and oxy-fuel atmosphere remain unchanged, regardless of the mechanism used.

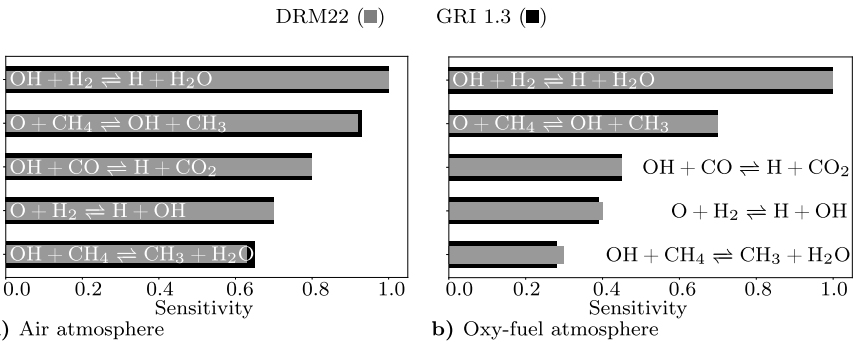

Fig. 9.5 Sensitivity of the average particle surface temperature with respect to the rates of gas-phase reactions of different mechanisms for air and oxy-fuel atmospheres

9.4.2 Sensitivities of Burning Rate

The burning rate, denoted by $\dot{m}_\mathrm{t}$, is a crucial QoI in particle combustion analysis. Similar to T_p, the burning rate is consistently increasing over time. Therefore, it is reasonable to define the time-averaged value of the burning rate as the QoI. This value can be defined as follows:

$$\mathrm{QoI} = \int_{\tau_0}^{\mathcal{T}} \dot{m}_\mathrm{t}\,\mathrm{d}\tau. \tag{9.28}$$

Rather than analysing the separate effects of char combustion and devolatilisation ($\dot{m}_\mathrm{t} = \dot{m}_\mathrm{c} + \dot{m}_\mathrm{v}$), it is possible to construct a QoI based on the variation of the total particle mass as shown in (9.13),

$$\mathrm{QoI} = \int_{\tau_0}^{\mathcal{T}} \dot{m}_\mathrm{t}\,\mathrm{d}\tau = -\int_{\tau_0}^{\mathcal{T}} \frac{\partial M_\mathrm{p}}{d\tau}\,\mathrm{d}\tau, \tag{9.29}$$

$$\mathrm{QoI} = -\int_{\tau_0}^{\mathcal{T}} \frac{\partial M_\mathrm{p}}{d\tau}\,\mathrm{d}\tau = M_\mathrm{p}|_{\tau_0} - M_\mathrm{p}|_{\mathcal{T}}, \tag{9.30}$$

This approach allows for a more comprehensive evaluation of the overall behaviour of the combustion process. The values of τ_0 and $\mathcal{T}$ are chosen to be similar to T_p in order to facilitate their comparison. Figure 9.6 displays the sensitivity analysis results with respect to the various system parameters. The sensitivity values for r_0 are significant, similar to that of the particle temperature, owing to the strong correlation between T_p and $\dot{m}_\mathrm{t}$. However, in contrast, the devolatilisation parameters have the most dominant effect when the char combustion rate is low, as $\dot{m}_\mathrm{t}$ is approximately equal to $\dot{m}_\mathrm{v}$, as there is no heterogeneous ignition. In comparison to the extracted sensitivities of particle temperature (Fig. 9.4), Fig. 9.6 indicates lower sensitivities for the thermodynamic parameters.

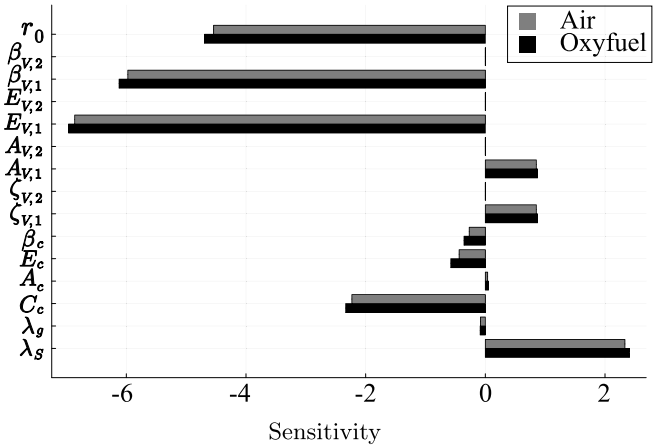

Fig. 9.6 Sensitivity of the average particle burning rate with respect to the particle parameters, for air and oxy-fuel atmospheres (reprinted from Hassan et al. [16], Copyright (2024), with permission from Elsevier and minor editing)

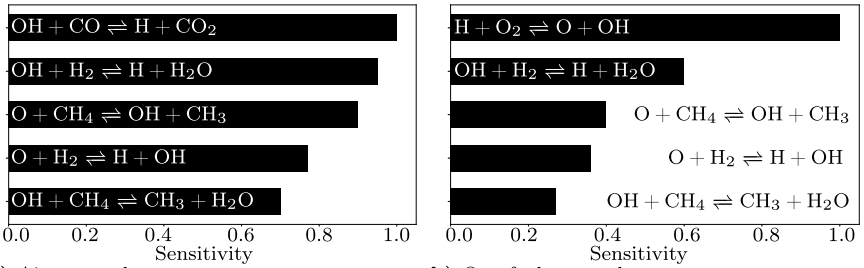

Fig. 9.7 Sensitivity of the average particle burning rate with respect to the rates of gas-phase reactions

Figure 9.7 highlights the sensitivities of the particle burning rate with respect to the gas-phase reaction rates. These results are consistent with the time-cumulative particle temperature results depicted in Fig. 9.5. The agreement is expected as the ignition process, particle temperature, and the burning rate are highly correlated in this setting. The only notable difference between Figs. 9.7a and 9.7b is that the reaction $OH + CO \rightleftharpoons H + CO_2$ is the most dominant in air atmosphere compared to oxy-fuel atmosphere. This is due to the high release rate of carbon dioxide in the air atmosphere, as shown in Fig. 9.2a.

9.5 Evolution of Sensitivities in Time

Given the unsteady nature of the problem, it is important to investigate the temporal evolution of sensitivities with respect to the most influential system parameters. In other words, instead of reporting sensitivities at a discrete time, as in the previous

sections, the evolution of these sensitivities for different time horizons needs to be reported. This information will allow to assess whether the predicted sensitivities depend on the time at which they are evaluated and, by definition, on the state of the time-varying system. This is achieved by adjusting the limits of the integral, for example in (9.27), to encompass the entire time domain of the QoI. The time domain is then discretised into several sequential segments, and the sensitivities are computed individually for each segment and then aggregated to provide the complete time evolution. It should also be noted that the sensitivities are in fact the rate of change of the quantity of interest with respect to the parameter. This rate could be either negative, meaning an inverse relationship, or positive. In any case, what is important for this study is the value of this change, as it implies a strong dependency of the quantity of interest on the respective parameter.

9.5.1 Particle Temperature as QoI

The results of the evolution of particle parameter sensitivities, when considering particle temperature as the quantity of interest, are shown in Fig. 9.8. These results demonstrate that the sensitivity of particle temperature (T_p) with respect to surface heat conductivity (λ_s) for both air and oxy-fuel atmosphere increases until $t \approx 1.5$ ms. This is because the gradient between the adjacent gas layer and particle temperatures decreases significantly at this stage, minimising the effect of λ_s. Gas conductivity λ_g follows a similar trend but with a more rapid decay rate due to the propagation of the flame towards the particle surface (not shown here).

Both volatiles activation energy and temperature exponent, ($E_{\mathrm{v},1}$ and $\beta_{\mathrm{v},1}$), show a similar behaviour independent of the atmosphere (air/oxy-fuel). They begin to have an impact after the early non-linear heating phase, close to the gas-phase ignition onset, as demonstrated in Fig. 9.2a. The sensitivities to particle radius and thermal capacity (r_0 and C_c, respectively) increase in both atmospheres as the heating rate of the particle $\frac{\mathrm{d}T_\mathrm{p}}{\mathrm{d}t}$ reaches its maximum. Following the ignition onset, their sensitivities decrease slightly as the heating rate of the particle diminishes and the flame spreads towards the particle surface.

9.5.2 Burning Rate as QoI

Evolution of particle burning rate sensitivities in time with respect to the top sensitive parameters is depicted in Fig. 9.9. Similar to particle temperature the sensitives of the dominant parameters reach their maximum when ignition occurs ($t = 1$ ms). These results are expected due to the strong impact of gas-phase ignition on devolatilisation rate and temperature gradient between the gas and particle surface. Comparison of Figs. 9.9 and 9.8 shows that the sensitivity of the temperature exponent $\beta_{\mathrm{v},1}$ in the devolatilisation model with respect to burning rate remains nearly constant regardless of the atmosphere. However, it exhibits a higher sensitivity value when compared to particle temperature.

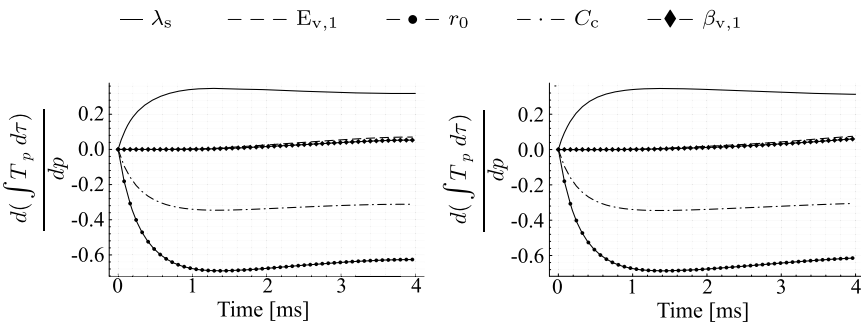

a) Air atmosphere **b)** Oxy-fuel atmosphere

Fig. 9.8 Temporal evolution of the average particle temperature sensitivities with respect to the system parameters (reprinted from Hassan et al. [16], Copyright (2024), with permission from Elsevier and minor editing)

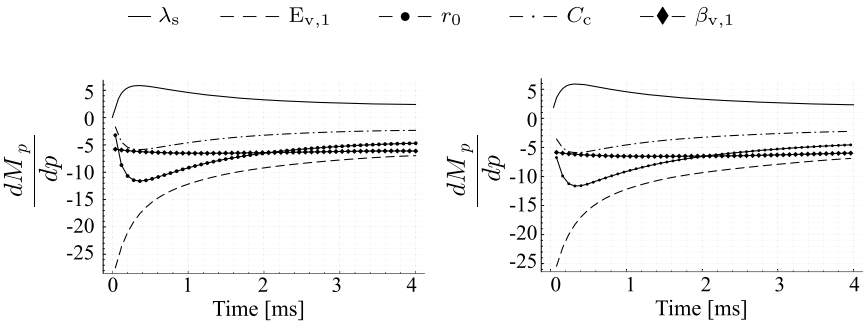

a) Air atmosphere **b)** Oxy-fuel atmosphere

Fig. 9.9 Temporal evolution of the average particle burning rate sensitivities with respect to the system parameters (reprinted from Hassan et al. [16], Copyright (2024), with permission from Elsevier and minor editing)

In both atmospheres, the particle burning rate is highly sensitive to the volatile activation energy $E_{v,1}$, especially at an early stage, where $\dot{m}_t \approx \dot{m}_v$ and char combustion is negligible. After gas-phase ignition, the particle temperature T_p becomes high enough and the sensitivity of the volatile activation energy dwindles with a similar rate independent of the atmosphere. It is worth noting that the signs of the sensitivities remain consistent and align with the findings presented in Fig. 9.6.

Comparison of Figs. 9.9 and 9.8 shows that while the atmosphere does not seem to influence the value and evolution of sensitivities with respect to different particle parameters, the selected QoI could have a large influence. This suggests that depending on the quantity to be predicted in such systems, different particle parameters could be influential, and how influential depends on the time instance that the analysis is performed.

9.6 Uncertainty Quantification

This section provides a brief description of the adjoint-based active subspace method (AASM), used to identify the dominant directions in the parameter space and to construct the resulting low-dimensional response surface.

The active subspace methodology aims to construct an M-dimensional subspace of the n-dimensional parameter space ($n \ll M$) that describes most of the variation of quantity of interest (QoI). The low-dimensional approximation of QoI is

$$\mathrm{QoI}(\mathrm{x}) \approx G(\mathrm{y}), \quad \mathrm{y} = \mathrm{S}^{\top}\mathrm{x} \tag{9.31}$$

where $G(\mathrm{y})$ is the response surface, $\mathrm{y} \in R^{M}$, $\mathbf{x} \in R^{n}$, and S is an orthogonal matrix. The active subspace is then defined as (S). One way to identify the active subspace is to perform an eigenvalue decomposition of the expectation matrix M defined as

$$\mathrm{M} = \frac{1}{N}\sum_{i=1}^{M}\left(\frac{\mathrm{dQoI}}{\mathrm{dx}_i}\right)\left(\frac{\mathrm{dQoI}}{\mathrm{dx}_i}\right)^{\top} = \mathrm{W}\boldsymbol{\Lambda}\mathrm{W}^{\top}, \tag{9.32}$$

where N denotes the number of samples, and W and $\boldsymbol{\Lambda}$ the eigenvalues and eigenvectors of the expectation matrix. Selecting the first R eigenvectors of this decomposition then constructs a reduced-order response surface G (y) that spans over the active dimensions. The gradients in (9.32) in turn are computed using the gradient extraction technique introduced in the previous section, leading to the adjoint-based active subspace method (AASM). The access to adjoint capabilities allows a cost effective method of extracting the required derivatives and has been shown in a previous study [15] to reduce the overall cost of the active subspace methodology considerably when applied to a zero-dimensional reactor. In this study, where a higher-dimensional configuration (i.e. axisymmetric particle) is considered, the gains are expected to be even more substantial.

To construct the response surface of a QoI with respect to the existing system parameters, the following steps are taken:

1. Choose the appropriate distribution for input variables
2. Assemble M random points of the input space, where $M = \eta \ln(D)$
3. Use adjoint-based method to compute the expectation matrix C from (9.32)
4. Apply eigenvalue decomposition to matrix C and choose the dominant eigenvalues and eigenvectors
5. Estimate upper and lower bounds for the eigenvalues with bootstrapping (vary M and repeat 3 and 4)
6. Construct the mapping matrix S from the dominant eigenvectors and compute the new variable $\mathrm{y} = \mathrm{S}^{\top}\mathrm{x}$
7. Construct the response surface $G(\mathrm{y}) \approx f(\mathrm{x})$ based on the number of active dimensions

For more details, regarding the algorithm see the study by Hassan et al. [15].

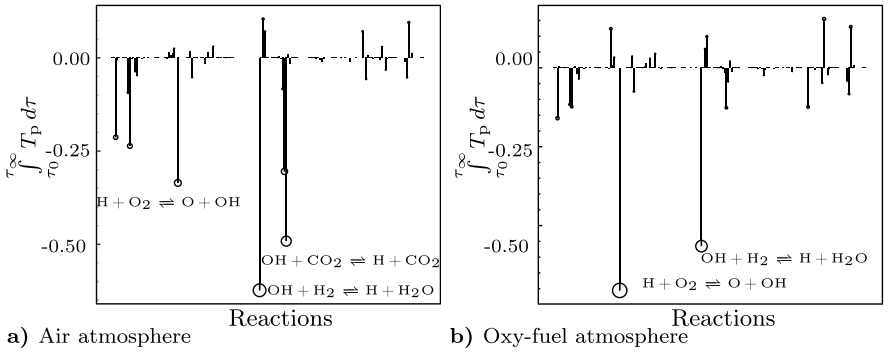

Fig. 9.10 Uncertainties of gas-phase reaction pathways for cumulative particle temperature (reprinted from Hassan et al. [16], Copyright (2024), with permission from Elsevier and minor editing)

9.6.1 Uncertainties in the Prediction of Particle Temperature and Burning Rate

As shown in the previous section and due to their impact on both particle temperature (T_p) and burning rate ($\dot{m}_t$), it is crucial to quantify the impact of uncertainties in gas-phase kinetics and particle parameters on the prediction of these quantities of interest. The uncertainties will be extracted as explained earlier. Due to the cost associated with the forward problem and gradient extraction, as well as the high accuracy of AASM, a total of 100 samples ($N = 100$) are utilised to construct the covariance matrix. A single dominant direction (the eigenvector related to the first eigenvalue) is picked to build the response surface of particle temperature T_p and the particle burning rate $\dot{m}_t$.

First the uncertainties with respect to the gas-phase kinetic models will be investigated. In this context, the dominant eigenvector is used as a representative of the dominant reaction pathway, shown in Fig. 9.10, using the average particle temperature as the QoI. These results can be directly compared to the results of the sensitivity analysis shown in Fig. 9.5. Figure 9.10 shows that $OH + H_2 \rightleftharpoons H + H_2O$ (R1) and $H + O_2 \rightleftharpoons O + OH$ (R2) are the most dominant reactions in air and oxy-fuel atmospheres, respectively, contributing significantly to the overall uncertainty of predictions.

It is worth noting that R2 also strongly contributes (within the top three reactions) to the predicted uncertainties of the air atmosphere. This is in contrast with the sensitivity analysis shown in Fig. 9.5a, where R2 ranks lower in the hierarchy of sensitive reactions. This highlights the limitation of a local method such as sensitivity analysis to analyse a complex system such as the one presented here. The reaction $OH + CO \rightleftharpoons H + CO_2$ remains important in the air atmosphere due to the elevated production of CO_2. This result is in alignment with the findings of the local sensitivity analysis in Fig. 9.5.

Finally, in order to examine the uncertainties of particle parameters on the overall predictions of the burning rate and particle temperature, a separate analysis is per-

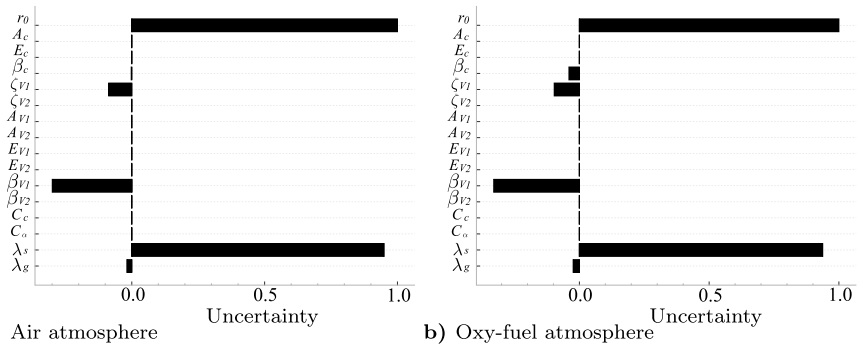

Fig. 9.11 Uncertainty of particle temperature with respect to particle parameters (reprinted from Hassan et al. [16], Copyright (2024), with permission from Elsevier and minor editing)

formed, where the kinetic parameters of gas-phase reactions are fixed and the AASM method is applied only on the samples extracted from the particle parameters shown in Figs. 9.4 and 9.6.

Since the number of selected particle parameters is smaller than the parameters of the gas-phase kinetic model, only 70 samples are used to build the response surface. The dominant eigenvectors, extracted using the AASM approach, highlighting the global sensitivity of particle temperature with respect to system parameters for each atmosphere are shown in Fig. 9.11 and can be compared directly to Fig. 9.4. When comparing global and local sensitivities, depicted in Figs. 9.11 and 9.4, respectively, it becomes evident that the particle radius r_0 emerges as the most sensitive parameter. Furthermore, the global sensitivity of particle thermal conductivity λ_s, as illustrated in Fig. 9.11, exceeds the sensitivity observed in the local analysis presented in Fig. 9.4. In contrast to the local sensitivity, Fig. 9.11 demonstrates minimal global sensitivity for particle thermal capacity C_c. Comparing Figs. 9.11a and 9.11b reveals that the global sensitivity remains consistent, irrespective of atmospheric conditions. These results are consistent with the findings from the local sensitivity analysis.

9.6.2 Evolution of Uncertainties in Time

However, as stressed previously, it is essential to assess the evolution of uncertainties over time in unsteady configurations. To accomplish this, the integration limits in (9.28) and (9.27) are sequentially changed from 0 to 5 ms. Figure 9.12 depicts the evolution of the predicted mean value and standard deviation, amplified 50 times for better visibility, superimposed. It reveals that the uncertainties are negligible during the heating phase regardless of the atmosphere and the QoI, and it becomes relatively more significant after the gas-phase ignition. This is because the gas-phase chemistry has minimal influence before the ignition onset. In addition, the uncertainties in the oxy-fuel atmosphere is consistently higher than that in the air atmosphere for all quantities of interest. Moreover, the uncertainties in the burning rate exceeds that of

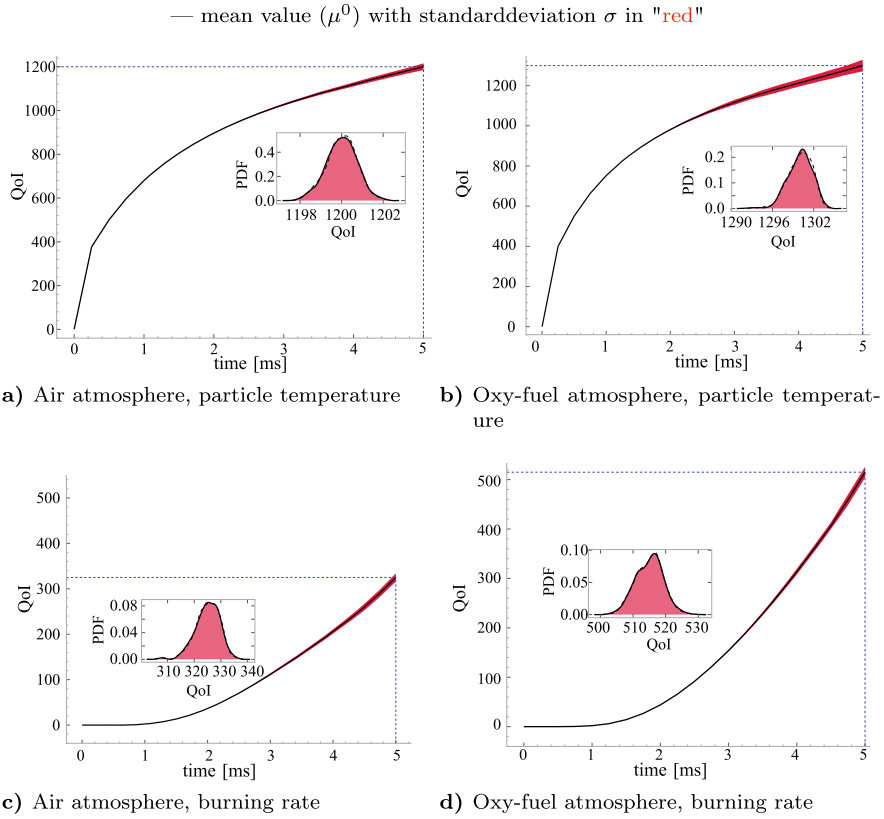

Fig. 9.12 Evolution of uncertainties in particle temperature and burning rate with respect to gas-phase kinetic parameters (reprinted from Hassan et al. [16], Copyright (2024), with permission from Elsevier and minor editing)

the particle temperature. This is attributed to the fact that the burned mass is more sensitive to gas-phase kinetics compared to the particle temperature.

Figure 9.13 displays the evolution of uncertainties in particle temperature and burning rate with respect to system parameters. By comparing Figs. 9.13 and 9.12, it is observable that system parameters have a much more substantial influence on uncertainties than the reactions rates. This can be attributed to the pre-ignition stage's primary role in controlling the particle's heating rate. Although the atmosphere has a negligible impact on sensitivities (Figs. 9.4 and 9.6), Fig. 9.13 demonstrates that the uncertainties in an oxy-fuel atmosphere are higher than those in an air atmosphere. Moreover, the uncertainties in the oxy-fuel atmosphere increase as ignition progresses, in line with the trends seen in reaction rate Fig. 9.12.

Uncertainties in the burning rate before ignition are almost negligible. However, these uncertainties become significantly more pronounced in both air and oxy-fuel atmospheres after ignition. Comparing the results of Fig. 9.13 reveals that the uncertainties in burning rate are much higher than those in particle temperature. This

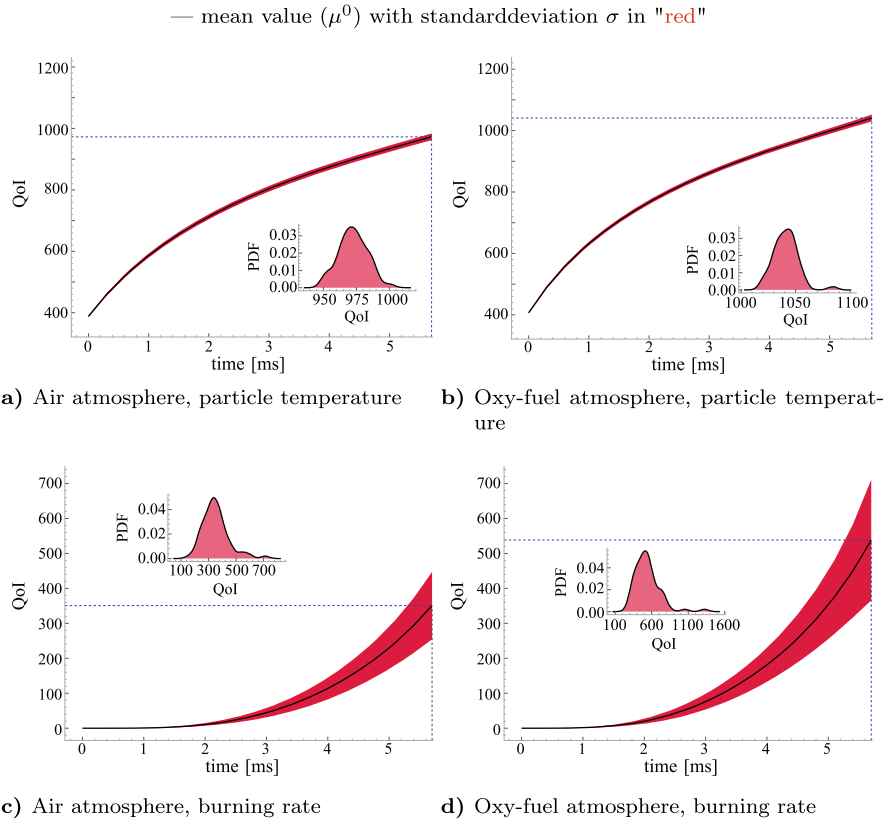

Fig. 9.13 Evolution of uncertainties in particle temperature and burning rate with respect to particle parameters (reprinted from Hassan et al. [16], Copyright (2024), with permission from Elsevier and minor editing)

suggests that particle burning rate is more globally sensitive to system parameters. Moreover, it is important to note that the results of the uncertainties are highly dependent on the uncertainty factor (UF). Therefore, even a small variation in the value of UF can significantly affect the evolution of uncertainties. Due to the shortage of reliable information regarding the value of the uncertainty factor for particle parameters, the chosen value is (UF = 1.1), as a further increase in this value of UF could lead to unrealistic results (not show here). Comparing Figs. 9.13 and 9.8 reveals that while the sensitivities of system parameters remain unaffected by the atmosphere, the uncertainties are significantly influenced by atmospheric conditions. This underscores the importance of performing uncertainty quantification in determining the influence of system parameters on prediction of different quantities of interest.

Comparing the different probability density functions (PDF) in Fig. 9.13 for particle temperature T_p and the average burning rate $\dot{m}_t$ reveals a higher skewness value for the $\dot{m}_t$ PDF compared to the T_p PDF. Furthermore, similar to PDF in Fig. 9.12,

the PDF for an oxy-fuel atmosphere exhibit higher skewness than those for an air atmosphere.

9.7 Conclusion

This chapter presents an overview of the sensitivity analysis and the uncertainty quantification of several models for solid fuel combustion, including char burnout, devolatilisation and detailed gas-phase kinetics. These models are applied in the simulation of an unsteady axisymmetric reacting particle. To determine the influence of the atmosphere, all the results were compared in both air and oxy-fuel atmospheres. The evolution of species shows that carbon dioxide levels increase in the air atmosphere compared to the oxy-fuel atmosphere due to the high rate of reaction $OH + CO \rightleftharpoons H + CO_2$. Analysing the particle burning rate reveals exponential growth after gas-phase ignition as the devolatilisation process becomes highly active, while the char combustion is negligible due to the limitation of oxygen accessibility to the particle surface. This result is valid for both air and oxy-fuel atmospheres.

To determine the most critical parameters, a semi-discrete adjoint approach is utilised. The resulting sensitivities showed that the particle size is the most influential parameter, regardless of the atmosphere (air/oxy-fuel), when considering the average particle temperature as the QoI. These results are consistent with the findings of [22]. However, when considering the average burning rate as the QoI, devolatilisation parameters become more significant due to the insignificant char combustion during the initial stage of devolatilisation. Additionally, analysis of the sensitivity of different quantities of interest with respect to gas-phase reaction rates indicated that volatile species play a vital role. Comparing the dominant reactions in air and oxy-fuel atmospheres shows that the reactions involving hydroxyl and hydrogen radicals are the most sensitive reactions.

By analysing the evolution of the sensitivities of the most dominant parameters over time, it is revealed that the maximum values occur during the early heating phase of the particle. Moreover, the sensitivity values for most parameters evolve until the onset of gas-phase ignition, at which point the sensitivity trend changes. However, the local gradient is not indicative of the actual reaction path, so the AASM is used to assess global sensitivities, as discussed in the study by Hassan et al. [15]. The reaction pathways were extracted to gain a global insight into the most effective reactions. High values were extracted for the $OH + H_2 \rightleftharpoons H + H_2O$ reaction in air atmosphere and the $H + O_2 \rightleftharpoons O + OH$ reaction in the oxy-fuel atmosphere.

Following the same analogies, the evolution of uncertainties for different quantities of interest (QoI) was extracted and compared. It is observed that there are negligible uncertainties during the heating up phase, but uncertainties gradually increase after the onset of gas-phase combustion. In the case of an oxy-fuel atmosphere, the uncertainties are larger compared to an air atmosphere due to higher gas-phase temperatures and earlier ignition. To validate these extracted uncertainties, probability density functions (PDF) of various quantities of interest related to gas-phase reaction rates at specific times were extracted.

Applying AASM in order to extract the global sensitivities of the particle temperature with respect to particle parameters reveals that the most dominant parameter is particle radius r_0 independent of the atmosphere. Also, the evolution of uncertainties in system parameters is analysed over time and compare them with the uncertainties in reaction rates. The comparison demonstrates that the uncertainties in reaction rates are negligible compared to those of system parameters. Additionally, similar to the uncertainties in reaction rates, the oxy-fuel atmosphere exhibits higher uncertainties than the air atmosphere. These findings highlight the higher influence of system parameters on various quantities of interest (QoI) in comparison to gas-phase chemical rates.

When comparing air and oxy-fuel atmospheres, the PDF reveal that the oxy-fuel atmosphere displays pronounced skewness and kurtosis owing to its heightened flammability and extended ignition delay time in gas-phase ignition, in contrast to the air atmosphere. This underscores the significance of investigating gas-phase ignition time and location.

Finally, it should be noted that among the parameters that could be influential in such analysis, initial temperature and pressure are also of great importance. While the impact of temperature on the burning rate has been previously demonstrated in the study by Hassan et al. [8], the analysis of the pressure effects has been left as part of future work, since the models used in this study are all calibrated for atmospheric pressure.

Acknowledgements This work has been funded by the Deutsche Forschungsgemeinschaft (DFG, German Research Foundation)—215035359—SFB/TRR 129 'Oxyflame'.

References

1. Pironneau, O. "On Optimum Design in Fluid Mechanics". *Journal of Fluid Mechanics* 64.1 (1974), 97–110. https://doi.org/10.1017/S0022112074002023
2. Jameson, A., Martinelli, L. and Pierce, N. A. "Optimum Aerodynamic Design Using the Navier-Stokes Equations". *Theoretical and Computational Fluid Dynamics* 10.1–4 (1998), 213–237. https://doi.org/10.1007/s001620050060
3. Fikl, A., Le Chenadec, V. and Sayadi, T. "Control and Optimization of Interfacial Flows Using Adjoint-Based Techniques". *Fluids* 5.3 (2020), 156. https://doi.org/10.3390/fluids5030156
4. Lemke, M., Cai, L., Reiss, J., Pitsch, H. and Sesterhenn, J. "Adjoint-Based Sensitivity Analysis of Quantities of Interest of Complex Combustion Models". *Combustion Theory and Modelling* 23.1 (2019), 180–196. https://doi.org/10.1080/13647830.2018.1495845
5. Braman, K., Oliver, T. A. and Raman, V. "Adjoint-Based Sensitivity Analysis of Flames". *Combustion Theory and Modelling* 19.1 (2015), 29–56. https://doi.org/10.1080/13647830.2014.976274
6. Kord, A. and Capecelatro, J. "A Discrete-Adjoint Framework for Optimizing High-Fidelity Simulations of Turbulent Reacting Flows". *Proceedings of the Combustion Institute* 39.4 (2023), 5375–5384. https://doi.org/10.1016/j.proci.2022.06.021
7. Hassan, A., Sayadi, T., Le Chenadec, V., Pitsch, H. and Attili, A. "Adjoint-Based Sensitivity Analysis of Steady Char Burnout". *Combustion Theory and Modelling* 25.1 (2021), 96–120. https://doi.org/10.1080/13647830.2020.1838614
8. Hassan, A., Sayadi, T., Le Chenadec, V. and Attili, A. "Sensitivity Analysis of an Unsteady Char Particle Combustion". *Fuel* 287 (2021). https://doi.org/10.1016/j.fuel.2020.119738

9. Eldred, M. and Burkardt, J. "Comparison of Non-Intrusive Polynomial Chaos and Stochastic Collocation Methods for Uncertainty Quantification". *47th AIAA Aerospace Sciences Meeting*. Orlando, Florida, USA, 2009. https://doi.org/10.2514/6.2009-976
10. Xiu, D. and Hesthaven, J. S. "High-Order Collocation Methods for Differential Equations with Random Inputs". *SIAM Journal on Scientific Computing* 27.3 (2005), 1118–1139. https://doi.org/10.1137/040615201
11. Li, H., Tang, Y., Ren, X., Xu, L. and Xu, X. "The Way to Develop Software Towards Exascale Computing". *Proceedings of the 2016 International Conference on High Performance Computing & Simulation*. Innsbruck, Austria, 2016, pp. 334–341.
12. Constantine, P. G., Dow, E. and Wang, Q. "Active Subspace Methods in Theory and Practice: Applications to Kriging Surfaces". *SIAM Journal on Scientific Computing* 36.4 (2014), A1500–A1524. https://doi.org/10.1137/130916138
13. Ji, W., Wang, J., Zahm, O., Marzouk, Y. M., Yang, B., Ren, Z. and Law, C. K. "Shared Low-Dimensional Subspaces for Propagating Kinetic Uncertainty to Multiple Outputs". *Combustion and Flame* 190 (2018), 146–157. https://doi.org/10.1016/j.combustflame.2017.11.021
14. Ji, W., Ren, Z., Marzouk, Y. and Law, C. K. "Quantifying Kinetic Uncertainty in Turbulent Combustion Simulations Using Active Subspaces". *Proceedings of the Combustion Institute* 37.2 (2019), 2175–2182. https://doi.org/10.1016/j.proci.2018.06.206
15. Hassan, A., Sabry, M., Le Chenadec, V. and Sayadi, T. "Uncertainty Quantification of Kinetic Models Using Adjoint-Driven Active Subspace Algorithms". *Proceedings of the Combustion Institute* 39.4 (2023), 5209–5218. https://doi.org/10.1016/j.proci.2022.07.177
16. Hassan, A., Schumacher, L., Sabry, M., Le Chenadec, V. and Sayadi, T. "Uncertainty Quantification and Sensitivity Analysis of an Unsteady Axisymmetric Reacting Solid Particle". *Combustion and Flame* 262 (2024), 113365. https://doi.org/10.1016/j.combustflame.2024.113365
17. Farmand, P., Nicolai, H., Schumann, C., Attili, A., Berger, L., Li, T., Geschwindner, C., di Mare, F., Hasse, C., Böhm, B., Janicka, J. and Pitsch, H. "Numerical Investigation and Assessment of Flamelet-Based Models for the Prediction of Pulverized Solid Fuel Homogeneous Ignition and Combustion". *Combustion and Flame* 235 (2022), 111693. https://doi.org/10.1016/j.combustflame.2021.111693
18. Farazi, S., Sadr, M., Kang, S., Schiemann, M., Vorobiev, N., Scherer, V. and Pitsch, H. "Resolved Simulations of Single Char Particle Combustion in a Laminar Flow Field". *Fuel* 201 (2017), 15–28. https://doi.org/10.1016/j.fuel.2016.11.011
19. Du, X. and Annamalai, K. "The Transient Ignition of Isolated Coal Particle". *Combustion and Flame* 97.3–4 (1994), 339–354. https://doi.org/10.1016/0010-2180(94)90025-6
20. McBride, B. J., Gordon, S. and Reno, M. A. *Coefficients for Calculating Thermodynamic and Transport Properties of Individual Species*. 1993.
21. Hassan, A., Sayadi, T., Schiemann, M. and Scherer, V. "Adjoint-Based Sensitivity Analysis of Char Combustion Surface Reaction Kinetics". *Fuel* 287 (2021). https://doi.org/10.1016/j.fuel.2020.119503
22. Gonzalo-Tirado, C., Jiménez, S., Johansson, R. and Ballester, J. "Comparative Study of Four Alternative Models for CO Oxidation Around a Burning Coal Char Particle". *Combustion and Flame* 161.4 (2014), 1085–1095. https://doi.org/10.1016/j.combustflame.2013.09.025